Direct measurement of chiral structure and transport in single- and multi-walled carbon nanotubes

Taoran Cui[1], Letian Lin[2], Lu-Chang Qin[1,2] and Sean Washburn[1,2,3,4,5]

[1] Dept Physics and Astronomy, University of North Carolina at Chapel Hill, Chapel Hill, NC 27599, USA
[2] Dept Applied Physical Sciences, University of North Carolina at Chapel Hill, Chapel Hill, NC 27599, USA
[3] Dept Computer Science, University of North Carolina at Chapel Hill, Chapel Hill, NC 27599, USA
[4] Dept Biomedical Engineering, University of North Carolina at Chapel Hill, Chapel Hill, NC 27599, USA

E-mail: sean@physics.unc.edu

Received 2 March 2016, revised 5 July 2016
Accepted for publication 15 August 2016
Published 16 September 2016

Abstract

Electrical devices based on suspended multi-wall carbon nanotubes were constructed and studied. The chiral structure of each shell in a particular nanotube was determined using nanobeam electron diffraction in a transmission electron microscope. The transport properties of the carbon nanotube were also measured. The nanotube device length was short enough that the transport was nearly ballistic, and multiple subbands contributed to the conductance. Thermal excitation of carriers significantly affected nanotube resistance at room temperature.

Keywords: nanoelectromechanical, nanotube, transport

(Some figures may appear in colour only in the online journal)

1. Introduction

Carbon nanotubes (CNTs) have been studied for more than two decades [1], especially single-walled carbon nanotubes (SWNTs) and double-walled carbon nanotubes (DWNTs), for their unusual physical properties. Each shell in any of these structures comprises a graphene lattice with C–C bond length a_0 wrapped according to chiral indices u and v. Theoretical models have been developed to characterize the electrical and mechanical properties of a CNT based on its atomic structure, i.e. on (u,v). Numerous experimental studies have been performed on SWNTs and DWNTs [2–5], not only to verify the theoretical predictions, but also to investigate their potential as promising candidates for novel materials. Only a few, however, were able to measure the electrical properties and to correlate them to the atomic structure of the CNT [6–8]. Multi-walled carbon nanotubes (MWNTs) remain less well understood due to the complexity of multiple shells as well as interaction between the neighboring shells.

Unlike other approaches to characterize CNTs, such as optical spectroscopy, atomic force microscopy, etc [9, 10], nano-beam electron diffraction (NBED) [11–14] is one of the most accurate and reliable techniques to reveal the atomic structure of a CNT, since more information can be interpreted from reciprocal space. In particular the chiral indices of each shell of a MWNT [15], which otherwise would be obscured by the outermost shell, can be determined for at least four shells. NBED is performed in a transmission electron microscope (TEM) because of the ability to converge the electron beam onto a small site, which is essential for a CNT due to its small size. The constraints of TEM, however, impose strict restrictions on the thickness of the specimen: the measured CNT has to be suspended from the substrate over an opening, which can be realized only with delicate nano-fabrication techniques. To circumvent the difficulty, in a few similar experiments that have been reported, CNTs were either randomly deposited on a sample holder

[5] Author to whom any correspondence should be addressed.

[16] or transferred to a TEM grid [8], however both of these were subject to low reproducibility and consequently produced a low yield.

In this work, we report on a sophisticated technique for fabrication of a nanoelectromechanical system (NEMS) based on a suspended CNT. We measure the transport properties and the chirality of the CNT and we discuss correlations between the two measurements. We also compare the experimental results with theoretical predictions for relevant transport mechanisms.

2. Experimental methods

Long and straight SWNTs, DWNTs, and few-walled carbon nanotubes (FWNTs) were grown by chemical vapor deposition using $Fe(NO_3)_2$, $FeSi_2$, and $(NH_4)_6Mo_7O_{24}/Co(NO_3)_2$ catalysts, respectively, on a 500 μm silicon substrate with Si_3N_4/SiO_2 layers of thickness 200 nm/200 nm on the top. The synthesis was controlled to produce a sparse distribution of CNTs of approximately 20 CNTs per mm^2.

Prior to CNT synthesis, the substrate was prepared by back-etching most of the Si out of a 1 mm $\times$ 1 mm window with KOH (15% : H_2O) at 70C [17]. After this step, a thin ($\simeq$ 100 nm) $Si/Si_3N_4/SiO_2$ membrane or 'window' remained. An additional SiO_2 layer was then deposited using plasma enhanced chemical vapor deposition (PECVD) on the top of the substrate to ensure that the top surface was insulated from the back contact. The window that remained supported CNTs during synthesis and subsequent sonication.

Chromium/gold bi-layer electrodes in the scale of 10μm–1 mm were patterned by standard photolithography on the top SiO_2 surface near the etched window. Any CNTs shorting the electrodes were then burned out with a high current. Palladium [18] leads of width 200 nm were selectively deposited to connect CNTs with the electrodes using electron beam lithography. The electrodes were all grounded to remove static charges throughout all subsequent steps. The CNT were annealed in flowing Ar:H_2 gas to improve contact between the Pd electrodes and CNT [19]. During measurements of the *I–V* characteristic of each CNT segment at room temperature electrodes were selectively connected to the measurement system, while others remained grounded.

To suspend a CNT for TEM imaging and NBED, HNA (a solution mixed with hydrofluoric acid, nitric acid and acetic acid), focus ion beam system (FIB) and hydrofluoric acid were sequentially applied to remove the remaining Si, Si_3N_4 and SiO_2 membranes beneath the target CNT [20]. Outside the etched window, both ends of the CNT segment were securely anchored by the Pd leads to minimize the mechanical vibration. In many samples, multiple segments of the same CNT were exposed over windows to allow control measurements. To avoid potential damage to the CNTs by high energy electrons, both real space images and NBED pattern were obtained with JEOL TEM 2010F at a relatively low voltage, 80 kV for SWNTs [21] and 120 kV for MWNTs, as a compromise between resolution and knock-out damage.

3. Results and discussions

Prior to the suspension, the CNTs were all horizontally aligned on the substrates. Due to their large Young's modulus of 1 TPa, the anchored CNTs remained straight during the NBED imaging despite possible small uniaxial strains [22], and the incident angle of electron beam remained approximately 90°. Therefore, any alteration due to the uniaxial deformation on the NBED pattern is negligible [11, 23, 24].

A systematic procedure has been established and practiced to identify the chirality of a CNT from analysis of the NBED pattern [12, 25, 26]. In general, real space TEM images first reveal the shell number of a CNT and the approximate diameter of each shell [27]. Auxiliary hexagons are drawn on NBED patterns to distinguish the principal layer lines L_1, L_2 and L_3 of each shell [28]. The ratio of chiral indices can then be determined as

$$\frac{v}{u} = \frac{2D_2 - D_1}{2D_1 - D_2} \tag{1}$$

where D_1 and D_2 are the spacings of the first and second principal layer lines from the equatorial line. Moreover, either chiral index of an individual shell can be calculated as the order of the Bessel function from the intensity profile of a specific principal layer line. In cases of ambiguity for layer line spacing combined with apparent diameter, the modeled Bessel function was compared directly with the diffraction intensity along the layer line to determine the particular choice of chiral indices [27]. The level of detail in the NBED pattern is subject to the resolution limit of the TEM and to the background noise, which can result in uncertainty in $\frac{v}{u}$ and hence in indistinct maxima along the intensity profiles. Hence, the chirality is confirmed by comparing the diameter of each shell computed using the chiral indices with the one measured in TEM images. We should note that, in the case of a MWNT, the more distal principal layer lines in the NBED pattern do not necessarily correspond to the larger shell.

Figure 1 shows the NBED pattern and the TEM image of a quadruple-walled carbon nanotube (QWNT). The ratio $\frac{v}{u}$ of each shell was measured as 0.274, 0.711, 0.634 and 1.000 from the outermost set of NBED patterns to the innermost one with an average uncertainty of 0.009, and the intensity profiles of each shell indicate the chiral indices $v = 16{,}17$, $u = 40{,}41$, $u = 35{,}35$ and $v = 19{,}20{,}21$ respectively. Combined with the diameters measured in the TEM image (inset figure 1, the most plausible chirality of the QWNT is determined as $(61, 17) : (40, 28) : (35, 22) : (21, 21)$. The chiral structures of the other CNT samples were identified with the same method. Details of the procedure to fit the indices are available in the literature [28, 29].

Figure 2 shows the typical *I–V* characteristics of both metallic and semiconducting SWNTs. The linearity at the low bias indicates a fairly ohmic (i.e. linear) contact between the CNT and the electrodes, which is expected due to the high work function of Pd and the low Schottky barrier. Table 1 summarizes the results from the NBED analysis and the transport experiments on the 17 CNT devices studied in this

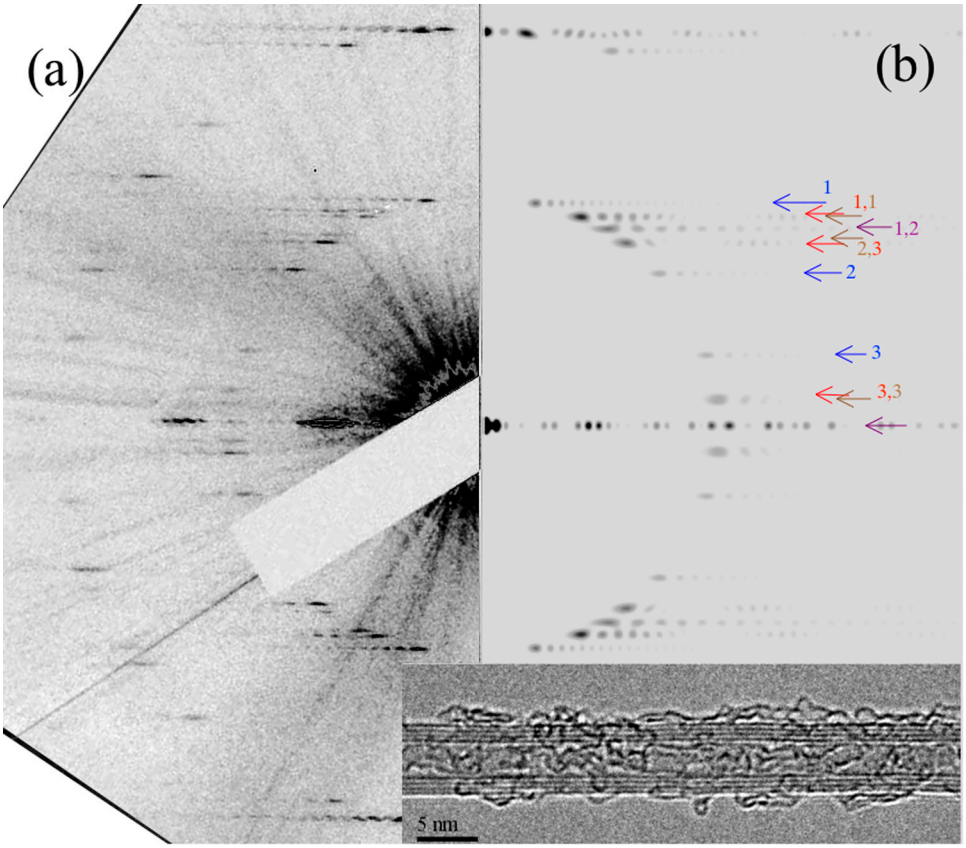

Figure 1. (a) NBED pattern of a QWNT consisting of the first and the second order of principal layer lines. (b) Simulated diffraction pattern of the QWNT with chiral indices for the four shells listed below. Layer lines for the model are marked with different colored indices. (inset) A real-space image of the QWNT. The diameter of the shells are 5.66 nm (blue), 4.66 nm (red), 4.06 nm (brown), and 3.25 nm (purple). These all have uncertainties of ±0.1 nm due to the TEM resolution limits.

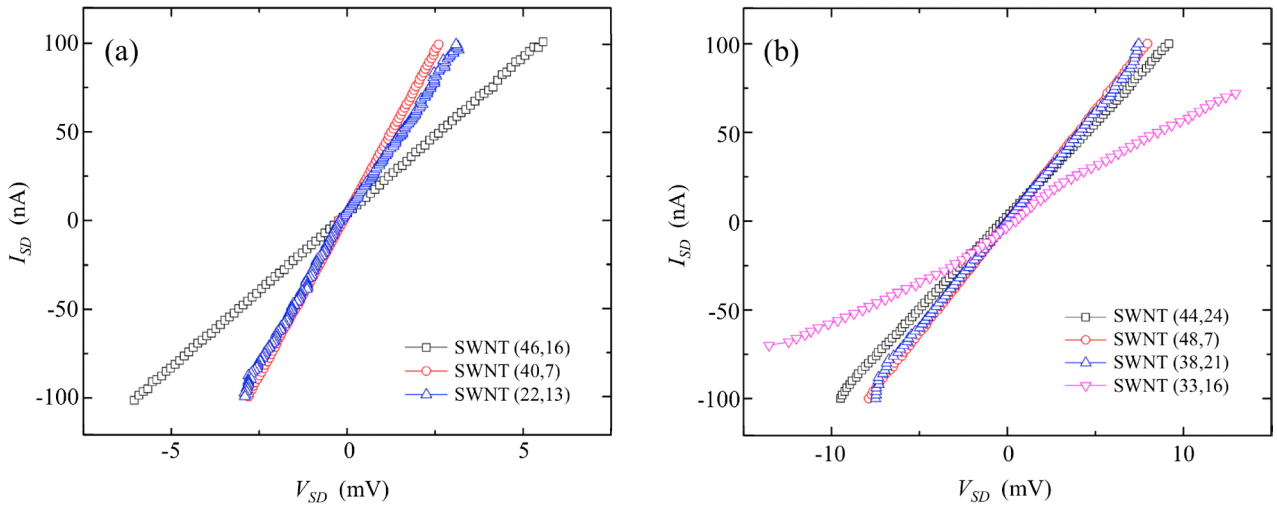

Figure 2. Representative source/drain current I_{SD} versus voltage V_{SD} for $T = 300$ K in (a) metallic and (b) semiconducting SWNT devices.

project. From table 1, we observe that the transport behavior of SWNTs agree with the theoretical classification based on the measured chiral indices $|u - v| = 3p + q$, where p is a integer and $q = \pm 1$ for semiconducting SWNTs and $q = 0$ for metallic ones. We also should note that several MWNTs comprise a metallic inner shell and a semiconducting outermost shell. The total resistances of these MWNTs are larger than the common resistances of metallic SWNTs, which indicates that the transport property of a MWNT is determined by the outermost shell in intimate contact with electrodes. Transport through a MWNT is expected to be the same as through a SWNT of the same chirality as the outermost shell, which is consistent with previous experiments [16, 30] and predictions [31].

It is necessary to determine in which transport regime our CNTs belong before attempting quantitative analysis of the

Table 1. Summary of physical properties of CNTs, where L and R are measured CNT conducting length and the corresponding resistance with low DC bias.

#	(u,v)	d (nm)	E_g (eV)	S/M	L (μm)	R (kΩ)
1	(46,16)	4.37	0.001	M	0.90	56
1	(40,7)	3.44	0.001	M	0.57	25
1	(22,13)	2.40	0.006	M	0.60	30
1	(44,24)	4.68	0.147	S	0.70	86
1	(48,7)	4.06	0.169	S	0.61	85
1	(38,21)	4.06	0.170	S	0.62	80
1	(85,10)	7.08	0.000	M	0.58	45
1	(33,16)	3.39	0.204	S	0.62	156
2	(27,22)	3.33	0.208	S	0.63	223
	(30,7)	2.67	0.258	S		
2	(38,6)	3.24	0.212	S	0.65	240
	(19,19)	2.58	0.005	M		
2	(48,21)	4.80	0.001	M	0.63	48
	(43,15)	4.09	0.168	S		
2	(40,12)	3.69	0.186	S	0.62	90
	(28,15)	2.96	0.234	S		
2	(54, 11)	4.72	0.145	S	0.53	60
	(47, 8)	4.03	0.001	M		
2	(49, 18)	4.71	0.146	S	0.62	76
	(36, 14)	3.50	0.197	S		
	(53, 7)	4.45	0.154	S		
3	(42, 8)	3.64	0.188	S	0.58	80
	(28, 11)	2.73	0.253	S		
	(47, 13)	4.28	0.160	S		
3	(32, 20)	3.56	0.003	M	0.71	114
	(29, 22)	3.47	0.199	S		
	(61, 17)	5.57	0.012	S		
4	(40,28)	4.64	0.002	M	0.59	65
	(35, 22)	3.90	0.177	S		
	(22,22)	2.99	0.004	M		

Note: # is the number of shells. (u,v) and d are the chiral indices and the diameter of a CNT as determined from the NBED patterns, E_g is the calculated band gap. S/M indicates whether a SWNT or an individual shell of a MWNT is semiconducting or metallic.

transport properties. Figure 3 shows a typical dependence of the measured resistance R of a SWNT on the length L between the probes. Here we follow methods developed previously [32]. The intercept suggests that the total contact resistance is 30 kΩ, and the slope indicates a 1D resistivity $\rho = \frac{dR}{dx}$ of approximately 4.5 kΩ μm^{-1}. From this measurement, the mean free path of the system is calculated [33] as $L_m \approx 2$ μm. Similar values were measured in various CNTs, and hence it is valid to assume that the transport in the CNTs in table 1 was quasi-ballistic, since the conducting lengths L of CNTs were in the range of 0.5–0.9 μm, i.e. smaller than the mean free path.

Once the chirality of a CNT is determined, we are able to construct the band structure in the reduced zone scheme. Given the diameters of the CNTs we measured were larger than 2 nm, the modification of the graphitic bands due to the orbital hybridization is not large. The band gap E_g can be calculated from [34–36]

$$E_g \simeq \frac{\eta 2a_0|V_{pp\pi}|}{d}\left[1 + (-1)^p \frac{2\gamma}{d}\cos(3\theta)\right], \qquad (2)$$

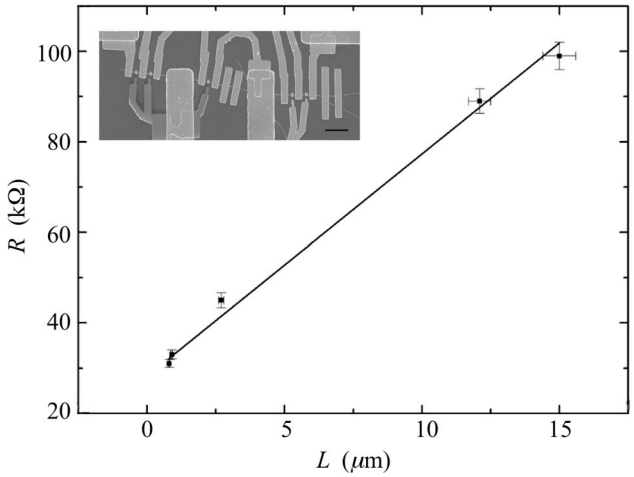

Figure 3. Low bias resistance $R = (dV_{SD}/dI_{SD})$ near zero bias as a function of conducting length L of the SWNT shown in a SEM image (inset). This is a metallic SWNT with $(u,v) = (22,13)$. The scale bar represents 4 μm.

where the chiral angle θ, $p = |u - v| \bmod 3$, $\eta = 1 - 1.6a_0^2/d^2$, $\gamma = 0.40$ are parameters arising from the structure of the particular shell, and $V_{pp\pi} = -2.24$ eV is the tight-binding overlap integral for π orbitals on nearest neighbors [37]. For shells like ours with larger diameters ($d > 2$ nm), the first term is sufficient to describe the gap in semiconducting CNTs. Many theoretical studies have concentrated on small diameter SWNTs, which have either only one Dirac point or a bandgap of order 100 meV at the Fermi surface. In that case it is valid to assume that the transport and the probability of thermal excitation of a semiconducting SWNT at room temperature is low. Simple armchair or zig-zag SWNTs are rare in reality. All of the CNTs we found in this study were chiral except a small minority of inner shells of a DWNT and a QWNT. Generally, each metallic SWNT has around 10 Dirac points in the vicinity of the Fermi surface within the first BZ, which suggests that around 20 channels are contributing to the conductance, the nearest subbands are separated by 0.4 eV. On the other hand, both the bandgap and the energy difference between the second nearest subbands in a semiconducting SWNT are comparable to the thermal energy at room temperature because of the relatively large diameters. Therefore the thermal excitation and the multiple band conduction must be taken into account when analyzing the transport properties. We acknowledge that the values above are approximations, but invoking them allows us to compare the resistance (or resistivity) with the band gap.

In the ballistic limit, the low bias resistance of a CNT device can be derived from Landauer–Büttiker formula as [38],

$$R = R_c + \frac{1}{|t|^2}\frac{h}{4e^2}\frac{1}{N}\left[1 + \exp\left(\frac{E_g}{2kT}\right)\right], \qquad (3)$$

where $|t|^2$ is the probability of electron transmission across the band gap, R_c is any excess contact resistance between the Pd electrodes and the CNT, and kT is the thermal energy. Figure 4 contains the measured short segment resistances plotted against the band gap values calculated from the

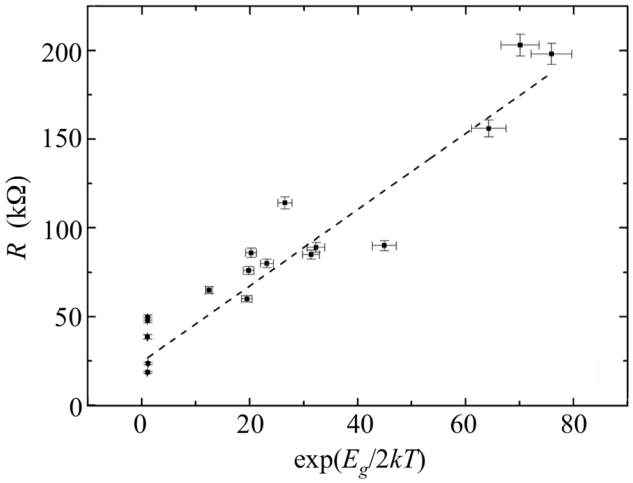

Figure 4. Dependence of the measured short-segment resistance R on the band gap E_g calculated from the measured u,v indices at room temperature $T = 300$ K.

measured chiral indices. The best fit yields a contact resistance $R_c = 30\,\mathrm{k}\Omega$ and the product of the channel count and the the transmission probability $N|t|^2 = 3.0$. If we invoke the average value of $N = 16$ for the whole population of CNT, this leads to a transmission probablility $|t|^2 = 0.2$, which is consistent with the results reported in other studies [22, 39]. These values are again approximate, but the trend of the gap dependence of the resistance is as expected in spite of the approximations.

4. Conclusion

In this work we have reported a technique to fabricate a suspended CNT, which allows the application of NBED to determine the chirality of individual shells of MWNT including the inner shells up to at least four nested shells. With the measured structural information in hand, we are able to correlate the predicted band structure of a specific CNT with its measured transport behavior. We concluded that the CNTs in our experiments behaved quasi-ballistically at room temperature, and that thermal excitation of carriers in large diameter semiconducting CNTs should be taken into account due to the small energy gaps. The modified Landauer–Büttiker formula successfully described the dependence of resistance on energy gap. This method will allow us to explore the physical and structural correlations of CNT characterized for chiral structure, and to investigate the effects of strain, doping, structural defects, and encapsulation. Measurements of large numbers of individual CNT samples also allowed direct comparison with the predicted and measured resistances of nanotubes.

Acknowledgments

The authors would like to thank Jie Liu at Duke University for help in CNT synthesis, and Jianping Lu for helpful discussions. We are also very grateful to the National Science Foundation Division of Electrical, Communications and Cyber Systems for funding.

References

[1] Iijima S and Ichihashi T 1993 Single-shell carbon nanotubes of 1 nm diameter *Nature* **363** 603–5
[2] Bockrath M, Cobden D, McEuen P, Chopra N, Zettl A, Thess A and Smalley R 1997 Single-electron transport in ropes of carbon nanotubes *Science* **275** 1922–5
[3] Yao Z, Kane C L and Dekker C 2000 High-field electrical transport in single-wall carbon nanotubes *Phys. Rev. Lett.* **84** 2941–4
[4] Javey A, Guo J, Paulsson M, Wang Q, Mann D, Lundstrom M and Dai H 2004 High-field quasiballistic transport in short carbon nanotubes *Phys. Rev. Lett.* **92** 106804
[5] Charlier J-C, Blase X and Roche S 2007 Electronic and transport properties of nanotubes *Rev. Mod. Phys.* **79** 677–732
[6] Wildoer J W, Venema L C, Rinzler A G, Smalley R E and Dekker C 1998 Electronic structure of atomically resolved carbon nanotubes *Nature* **391** 59–62
[7] Chandra B, Caldwell R, Huang M, Huang L, Sfeir M, O'Brien S, Heinz T and Hone J 2006 Electrical transport measurements of nanotubes with known (n, m) indices *Phys. Status Solidi* **243** 3359–64
[8] Allen C, Elkin M, Burnell G, Hickey B, Zhang C, Hofmann S and Robertson J 2011 Transport measurements on carbon nanotubes structurally characterized by electron diffraction *Phys. Rev.* B **84** 115444
[9] Odom T W, Huang J-L, Kim P and Lieber C M 1998 Atomic structure and electronic properties of single-walled carbon nanotubes *Nature* **391** 62–4
[10] Jorio A, Saito R, Hafner J, Lieber C, Hunter M, McClure T, Dresselhaus G and Dresselhaus M 2001 Structural (n, m) determination of isolated single-wall carbon nanotubes by resonant Raman scattering *Phys. Rev. Lett.* **86** 1118–21
[11] Gao M, Zuo J, Twesten R, Petrov I, Nagahara L and Zhang R 2003 Structure determination of individual single-wall carbon nanotubes by nanoarea electron diffraction *Appl. Phys. Lett.* **82** 2703–5
[12] Qin L-C 2006 Electron diffraction from carbon nanotubes *Rep. Prog. Phys.* **69** 2761
[13] Hirahara K, Inose K and Nakayama Y 2010 Determination of the chiralities of isolated carbon nanotubes during superplastic elongation process *Appl. Phys. Lett.* **97** 051905
[14] Lin L, Cui T, Qin L-C and Washburn S 2011 Direct measurement of the friction between and shear moduli of shells of carbon nanotubes *Phys. Rev. Lett.* **107** 206101
[15] Liu Z, Zhang Q and Qin L-C 2005 Accurate determination of atomic structure of multiwalled carbon nanotubes by nondestructive nanobeam electron diffraction *Appl. Phys. Lett.* **86** 191903
[16] Kociak M, Suenaga K, Hirahara K, Saito Y, Nakahira T and Iijima S 2002 Linking chiral indices and transport properties of double-walled carbon nanotubes *Phys. Rev. Lett.* **89** 155501
[17] Seidel H, Csepregi L, Heuberger A and Baumgartel H 1990 Anisotropic etching of crystalline silicon in alkaline solutions *J. Electrochem. Soc.* **137** 3612–26
[18] Mann D, Javey A, Kong J, Wang Q and Dai H 2003 Ballistic transport in metallic nanotubes with reliable Pd ohmic contacts *Nano Lett.* **3** 1541–4
[19] Javey A, Guo J, Wang Q, Lundstrom M and Dai H 2003 Ballistic carbon nanotube field-effect transistors *Nature* **424** 654–7
[20] Lin L 2011 Fabrication, structure and properties of a single carbon nanotube-based nano-electromechanical system *PhD Thesis* UNC-CH
[21] Smith B W and Luzzi D E 2001 Electron irradiation effects in single wall carbon nanotubes *J. Appl. Phys.* **90** 3509–15

[22] Minot E, Yaish Y, Sazonova V, Park J-Y, Brink M and McEuen P L 2003 Tuning carbon nanotube band gaps with strain *Phys. Rev. Lett.* **90** 156401
[23] Liu Z and Qin L-C 2004 Symmetry of electron diffraction from single-walled carbon nanotubes *Chem. Phys. Lett.* **400** 430–5
[24] Hirahara K, Kociak M, Bandow S, Nakahira T, Itoh K, Saito Y and Iijima S 2006 Chirality correlation in double-wall carbon nanotubes as studied by electron diffraction *Phys. Rev.* B **73** 195420
[25] Amelinckx S, Lucas A and Lambin P 1999 Electron diffraction and microscopy of nanotubes *Rep. Prog. Phys.* **62** 1471
[26] Liu Z and Qin L-C 2005 A direct method to determine the chiral indices of carbon nanotubes *Chem. Phys. Lett.* **408** 75–9
[27] Qin C and Peng L-M 2002 Measurement accuracy of the diameter of a carbon nanotube from TEM images *Phys. Rev.* B **65** 155431
[28] Deniz H, Derbakova A and Qin L-C 2010 A systematic procedure for determining the chiral indices of multi-walled carbon nanotubes using electron diffraction—each and every shell *Ultramicroscopy* **111** 66–72
[29] Cui T 2013 Structural and physical properties of torsional carbon nanotube devices by electron diffraction and microscopy *PhD Thesis* University of North Carolina at Chapel Hill
[30] Liu K, Wang W, Xu Z, Bai X, Wang E, Yao Y, Zhang J and Liu Z 2008 Chirality-dependent transport properties of double-walled nanotubes measured *in situ* on their field-effect transistors *J. Am. Chem. Soc.* **131** 62–3
[31] Yan Q, Wu J, Zhou G, Duan W and Gu B-L 2005 *Ab initio* study of transport properties of multiwalled carbon nanotubes *Phys. Rev.* B **72** 155425
[32] Purewal M S, Hong B, Ravi A, Chandra B, Hone J and Kim P 2007 Scaling of resistance and electron mean free path of single-walled carbon nanotubes *Phys. Rev. Lett.* **98** 186808
[33] Datta S 1997 *Electronic Transport in Mesoscopic Systems* (Cambridge: Cambridge University Press) (doi:10.1017/CBO9780511805776)
[34] Saito R, Dresselhaus G and Dresselhaus M 1993 Electronic structure of double-layer graphene tubules *J. Appl. Phys.* **73** 494–500
[35] Mintmire J W, Robertson D H and White C T 1993 Properties of fullerene nanotubeules *J. Phys. Chem. Solids* **54** 1835–40
[36] Yorikawa H and Muramatsu S 1995 Energy gaps of semiconducting nanotubes *Phys. Rev.* B **94** 086802
[37] Tomanek D and Schluter M 1991 Growth regimes of carbon clusters *Phys. Rev. Lett.* **67** 2331–4
[38] Cao J, Wang Q and Dai H 2003 Electromechanical properties of metallic, quasimetallic, and semiconducting carbon nanotubes under stretching *Phys. Rev. Lett.* **90** 157601
[39] Hall A R, Falvo M R, Superfine R and Washburn S 2007 Electromechanical response of single-walled carbon nanotubes to torsional strain in a self-contained device *Nat. Nanotechnol.* **2** 413–6